



# Experimental Determination of Optical and Structural Properties of Nanostructured SRO films Deposited by HFCVD and Theoretical Predictions By Global Reactions Model and DFT Method

## KEYWORDS

Global Reactions Model, luminescence, Silicon rich-Oxide, HFCVD and DFT.

N.D. Espinosa-Torres	A.D. Hernández de la Luz	J.F.J. Flores-Gracia
IC-CIDS Benemérita Universidad Autónoma de Puebla, C.U., Edif. 103 C-D, Col. San Manuel, C.P. 72570 Puebla, Pue., México.	IC-CIDS Benemérita Universidad Autónoma de Puebla, C.U., Edif. 103 C-D, Col. San Manuel, C.P. 72570 Puebla, Pue., México	IC-CIDS Benemérita Universidad Autónoma de Puebla, C.U., Edif. 103 C-D, Col. San Manuel, C.P. 72570 Puebla, Pue., México
J.A. Luna-López	J. Martínez-Juárez	
IC-CIDS Benemérita Universidad Autónoma de Puebla, C.U., Edif. 103 C-D, Col. San Manuel, C.P. 72570 Puebla, Pue., México	IC-CIDS Benemérita Universidad Autónoma de Puebla, C.U., Edif. 103 C-D, Col. San Manuel, C.P. 72570 Puebla, Pue., México	
D.E. Vázquez-Valerdi	A. Benítez-Lara	
IC-CIDS Benemérita Universidad Autónoma de Puebla, C.U., Edif. 103 C-D, Col. San Manuel, C.P. 72570 Puebla, Pue., México	IC-CIDS Benemérita Universidad Autónoma de Puebla, C.U., Edif. 103 C-D, Col. San Manuel, C.P. 72570 Puebla, Pue., México	

**ABSTRACT** This current work is devoted to present some important results obtained by theoretical calculations using DFT method and the Global Reactions Model (GRM) in relation to molecular structures and optical properties such as photoluminescence (PL), Fourier Transform Infrared (FTIR) spectroscopy and energy gaps  $E_g$  for silicon nanoclusters ( ) embedded in silicon rich oxide (SRO) films. We make comparisons between theoretical predictions and experimental results taking as reference experimental results obtained from measurements performed on SRO thin films obtained by the Hot Filament Chemical Vapor Deposition (HFCVD) technique. We stress that the scope of our theoretical predictions is general since it does not depend on the particular technique used to obtain the SRO structure but rather the suggested structure used in our GRM. As for main results found we have that a good correlation exists for  $E_g$  values in the case of films grown at 1020 °C corresponding to and molecular structures suggested as well as for films grown at 1150 °C in such case a molecular structure type  $Si_3O_9$  is associated. Regards PL correlation,  $SiO_x$  film grown at 900 °C gives a PL spectrum with two main peaks at 440nm and 548nm while theoretical spectrum shows peaks at 471nm and around of 549.8 nm and the corresponding molecular structure is type  $Si_7O_9$ . Besides, the same sample with a further annealing displays luminescence peaked at 405nm, 749nm and 820nm and in this case theoretical results predict only one correlated peak at 415nm using a molecule type . Also, in relation to the FTIR correlation, theoretical calculations predict frequencies of vibrational modes of bonds Si-O (rocking, bending, stretching) and Si-H (wagging, bending) whose value are well located in the experimental frequency range and Si-H the corresponding atomic structure is type .

## 1. Introduction

It is well known that the crystalline silicon has no photoluminescence due to multiple phenomena of non-radiative recombination between electrons and holes, and that the presents photoluminescence both by its amorphous nature and by their large gap. This latter property has been taken as a starting point to consider silicon confined systems of great in-terest because they offer the possibility of light emission from silicon-based materials. Following the initial report of the light emission from porous silicon, Canham in 1990, this has been a novel subject of intense scientific activity currently along with other confined systems. Particularly, from this latter, it results so important the Silicon Rich-Oxide (SRO) thin films. The physical microscopic structure of  $SiO_x$  is still a subject of discussion now-a-days, because its structural arrangement is a key knowledge to get a deep understanding about radiative emission mechanisms in this kind of nano-structured materials.

In the study of the SRO, one branch of research is focused on investigating the main mechanisms which generate the luminescent phenomena in this material. In the case of structures such as SRO thin films, it is found in litera-

ture different approaches. So, it has been proposed several mechanisms involved in the luminescent emission observed, these include among others: quantum confinement of excitons, luminescence due to chemical species (such as siloxanes, Silicon Oxides and Sub-oxides), interfacial states, defects and strain related luminescence. Although there is a growing consensus that the quantum confinement effects may explain some of the features of the luminescence spectra, it is clear that in some cases other important factors are present such as energy barriers, defects, size variations, geometrical arrangements and so on. Up to now, there are no complete models capable of including all mechanisms which are responsible of radiative emission.

On the other hand, luminescent phenomenon in SRO structures can be excited by different forms, so we find that experimentally, luminescence spectra are generated by Photo-Luminescence (PL), Electro-luminescence (EL) and Cathode-Luminescence (CL) mechanisms. The fundamental physical mechanism which explains correctly the origin of luminescent phenomena in each one of these different forms of excitation is still an active field of research.

Today, a few models are frequently used to describe a SRO network, namely: the Mixture Model (MM) by Bell and Ley, the Random Bonding Model (RBM) by Philipp, and the Intermediate Model (IM) introduced in 2011 by Novikov and Gritsenko. In 2012 Davor et al., in an extensive review, considered that the actual structure seems to be generally determined by the deposition procedure. In some works, the structures of films obtained by radio-frequency sputtering and physical evaporation were claimed to correspond to RBM, whereas the films obtained by magnetron-sputtering, plasma enhanced chemical vapor deposition (PECVD), have been assigned to MM. IM was used to describe layers prepared by Low Pressure Chemical Vapor Deposition (LPCVD) technique using SiH<sub>4</sub> and N<sub>2</sub>O as reactant precursors at 750 °C. Finally, we find a new model, the Global Reactions Model (GRM) suggested lately by Espinosa-Torres et al. This model describes, firstly the compulsory Global and Partial Reaction(s) to produce the oxide matrix and secondly, the annealing reactions for elucidating the compositional changes before and after the thermal annealing and subsequently the variations in the intensity of luminescence spectra and also, it describes a set of secondary reactions of the oxide matrices with the hydrogen produced in the reaction chamber to obtain the charged species that could be associated to the emission in SRO thin films with explicit defects.

On the other hand, among the different techniques used for depositing thin films we can mention the Hot Filament Chemical Vapor Deposition (HFCVD) technique. This technique is known by different names like I-CVD (initiated-CVD), Cat-CVD (Catalytic-CVD) and HWCVD (Hot Wire-CVD). Amorphous and micro-crystalline silicon could also be obtained with this method.

Another technique is that known as Low Pressure Chemical Vapor Deposition (LPCVD), it allows getting silicon-rich oxide layers using oxide species like nitrous oxide and silane compounds (silane) as reactants. Silicon excess is easily controlled by changing the partial pressure ratio  $R_o$  between N<sub>2</sub>O and SiH<sub>4</sub> defined by  $R_o = P(N_2O)/P(SiH_4)$  or simply  $R_o = N_2O/SiH_4$ .

In regard to the origin of the PL emission in Si-NCs, it is still a subject of debate; however we can find some proposals of models suggested explaining this phenomenon. One of these models relates the PL to Quantum Confinement Effects (QCE), the other model relates the PL to defects in the oxide matrix at the interface SiO<sub>2</sub>/Si-NCs. Broadly, both common accepted proposals make use of approximated quantum methods in order to solve the Schrödinger equation associated with quantum confinement of the electron restricted to move in so small spatial dimensions, hence their predictions about luminescent phenomenon are limited. Considering this important fact, we hope that an analysis of this phenomenon made from the view point of composition and molecular structures can significantly contribute to a better knowledge of luminescence in SRO considered as an arrangement of Si-NCs embedded in oxide matrices. The aim of this work is focused on theoretical predictions about PL, FTIR and energy gaps  $E_g$  of SRO thin films based on DFT method and the GRM. We make correlations with experimental results provided by measurements from SRO thin films obtained experimentally by Hot Filament Chemical Vapor Deposition (HFCVD) technique. Besides, by using the GRM and the DFT method we simulate nanoclusters of type Si<sub>n</sub>O<sub>n</sub> with  $5 < n < 18$  which may be found in SRO films in order to study their optical properties as well as their atomic structures which

give information about geometrical arrangements and their evolution with temperature effects. Comparisons with experimental results are made in order to point out that our theoretical predictions have contributed to understand in depth the origin of underlying luminescent mechanism in SRO nanostructures.

This paper is organized as follows. Section 2 presents the GRM, Section 3 presents results about theoretical predictions and comparisons with experimental results and Section 4 presents the main conclusions.

## 2. Global Reactions Model (GRM)

In this section we present a new mode which considers the compulsory Global and Partial Reaction(s) which are necessary to generate the oxide matrices (SiO<sub>2</sub>, Si<sub>2</sub>O<sub>3</sub>, SiO and Si<sub>2</sub>O) the annealing reactions for explaining the compositional changes before and after the thermal treatment and consequently the changes in luminescence spectra intensity and a set of secondary reactions of the oxide matrices with the hydrogen produced to obtain the ions that could be associated to the emission in SRO thin films with specific defects. When SRO is prepared by LPCVD, a gas mixture of and is habitually used, and the excess Si content can be modified by the gas flow ratio. The silicon excess can be as high as 17% for  $R_o=3$ ; and experimentally stoichiometric (a non-free silicon film) can be obtained for  $R_o > 50$ . Theoretically, corresponds to the stoichiometric silica, when a mixture silane-nitrogen 5 at% is used. Experimentally, there is enough evidence that SRO thin films are constituted by a silicon oxides mixture and not only by one of them, independently of the value of. We can establish the global reactions of the chemical combination of, and which generates the theoretical composition of SRO given by

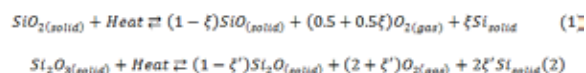
$$SiO_2 = (1-x)/(4+z+v), Si_2O_3 = (1-v)/(4+z+v), SiO = (1-y)/(4+z+v),$$

$$Si_2O = (1-z)/(4+z+v), Si = (x+y+2z+2v)/(4+z+v),$$

Where the parameters satisfy the conditions and.

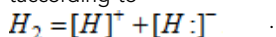
$$0 \leq x + y + 2z + v \leq 1.0.$$

When SRO thin films are annealed, some oxides are degraded. The plausible "annealing reactions" proposed are:



Double arrow stands for denoting equilibrium condition,  $\xi$  and  $\xi'$  are the progress of the annealing reactions. The extent of progress of reaction is defined as the ratio between the total change in the number of moles of a species and their stoichiometric coefficients.

As is known, a mole of any substance contains the number of atoms equal to the Avogadro's number. In order to perform first-principles calculations, the problem must be modeled with a maximum of 100 atoms, consequently the oxides must be rewritten in terms of the number of atoms, i.e.: Si<sub>2n</sub>O<sub>2n</sub>, Si<sub>2n</sub>O<sub>2n-3n</sub>, Si<sub>n</sub>O<sub>n</sub>, Si<sub>2n</sub>O<sub>n</sub>. The hydrogen gaseous can react according to



The hydrogen ion formed, in turn, reacts with the silicon

oxides to form ions such as, [Si<sub>n</sub>O<sub>2n</sub>H]<sup>+</sup>, [Si<sub>n</sub>O<sub>2n</sub>H]<sup>2+</sup>, etc. During heat treatment the reactions produce a dehydration of these cations, resulting in the formation of new ones, for

example,  $[Si_xO_{2x}H_2]^{2+} \in [Si_xO_{2x-1}]^{2+} + H_2O \uparrow$  and so on. Finally, the moieties obtained from these reactions result as:  $[Si_xO_{2x-1}]^{2+}, [Si_{1-x}O_{2x-1}]^{2+}, [Si_xO_{x-1}]^{2+}, [Si_{1-x}O_{x-1}]^{2+}$

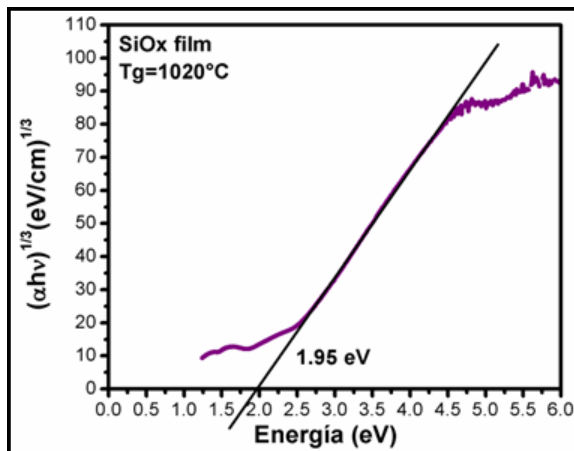
These anions formed are different oxides matrices containing vacancies or defects of silicon which may or not be present in the films of SRO.

**3. Results and discussion**

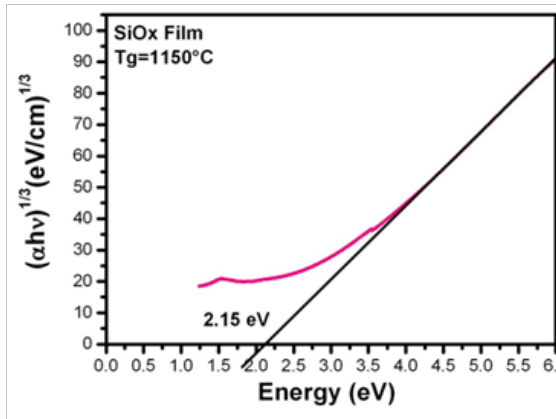
**3.1 Theoretical measurement of band gaps  $E_g$  for thin films considering the presence of structures and comparisons with experimental values.**

We display and discuss the results employing DFT for evaluating theoretically structures type  $Si_nO_n$ , where  $n$  is the number of silicon atoms. The GRM already discussed is employed to explain the physical microscopic structure of SRO thin films regardless of the technique used to obtain the SRO structure since we are only interested in its molecular composition and atomic arrangement.

We begin by taking  $SiO_x$  films obtained by HFCVD technique from our experimental group (results not even published). The approximate experimental values of the energy band gap are obtained by the relationship known as Tauc plot as shown in Figure 1. The methodology for obtaining the  $E_g$  has been described in a previous work. It is found that  $E_g$  decreases when the substrate temperature is raised. The band gap of the films lies in the range of 1.8-2.5 eV. When decreases out from 2.0 in (amorphous oxide), the valence band edge moves up, as the increased Si-Si bond states are gradually overlapped with the Oxygen Non-bonding States (ONS), and finally spread out into the Si valence band. Simultaneously, the conduction band edge also moves down, giving rise the band gap decreases nonlinearly when increasing continually the Si concentration.



(a)



(b)

**Figure 1. Determination of  $E_g$  for a film by making use of the relationship known as Tauc plot.  $[\alpha(h\nu)]^{1/3}$  versus energy ( $h\nu$ ) for two temperatures (a)  $T_g = 1020^\circ C$  and (b)  $T_g = 1150^\circ C$ .**

In Figure 1, we observe that making an extrapolation through the straight line according to Tauc procedure, we obtain the approximated band gaps which have values of 1.95 eV (upper part) and 2.15 eV (lower part). At first glance, the variations of  $E_g$  are originated by the difference in temperatures then it gives rise that  $E_g$  reduces as temperature increases. These two experimental values of  $E_g$  fit well with those obtained theoretically using DFT as shown in Table 1 which displays results for structures type  $Si_nO_n$ .

**Table 1. HOMO, LUMO and HOMO-LUMO Gap calculated using DFT for structures with .**

Number of silicon atoms	HOMO eV	LUMO eV	GAP eV
5	-6.19	-3.14	3.05
6	-6.01	-3.46	2.55
8	-5.51	-3.58	1.93
9	-5.34	-3.28	2.06
11	-5.93	-3.22	2.71
12	-5.97	-2.96	3.01
13	-5.61	-3.30	2.31
14	-6.04	-2.79	3.25
15	-6.11	-3.39	2.72
16	-6.16	-4.20	1.96

We have seen that thin films, deposited at , resulted with a band gap of 1.95 eV, calculated using Tauc technique. Now, by observing Table 1, we can correlate two possible theoretical values either corresponding to  $Si_8O_8$  molecule or corresponding to  $Si_{16}O_{16}$  one, existing the possibility of a mixture of them. On the other hand, film deposited at 1150°C correspond to an approximated experimental band gap of 2.15 eV which correlates well with a theoretical

calvalue of associated to  $\text{Si}_9\text{O}_9$  molecule in accordance with Table 1.

### 3.2 Theoretical PL spectra of the thin films and comparisons with experimental results.

Now, we proceed to our analysis in relationship to PL phenomenon. We show the results of the evaluation of structural and optical properties for a wide set of moieties, seemingly found in SRO. DFT results predict emission in visible region for molecules with a number of atoms less than 14 silicon ones. Results obtained in this research predict luminescence in visible region for just about half calculated structures, especially for silicon atoms, while large structures with display luminescence in ultraviolet region.

Inspecting, in Figure 2, the experimental IPL spectrum measured from the films grown at , we locate two emission bands both covering a wide spectral range from 380 to 750 nm (from violet to red).

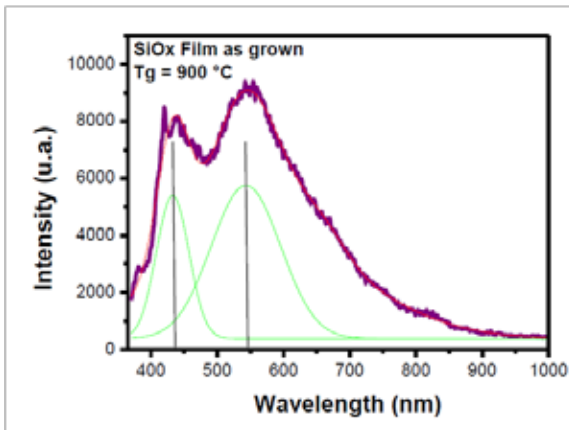


Figure 2. Experimental PL spectrum from a film grown at 900 °C.

The left band with a wide peak around 440 nm while the right one peak around 548 nm as can be confirmed by de-convolution curves. After making a further annealing to the same film, the PL spectrum (Figure 4) displays two main bands, one is the A band which lies in the violet-blue range (380-495 nm) peaked at 405 nm with a relatively weak PL intensity. The other band is the B one which lies in the orange-near infrared range (590-875 nm), this band shows a strong intensity and two main peaks, one located at 749 nm and other at 820 nm as confirmed again by de-convolution curves.

Looking at Figure 2 and Figure 4 and making comparisons between them, we infer that the PL intensity decreases after thermal annealing due to the PL intensity is lower after a further annealing. According to this result, we conclude that annealing process stimulates the formation of crystalline silicon (c-Si) as well as the formation of defects both contributing to the PL emission. For this reason the PL spectrum shifts to the red region.

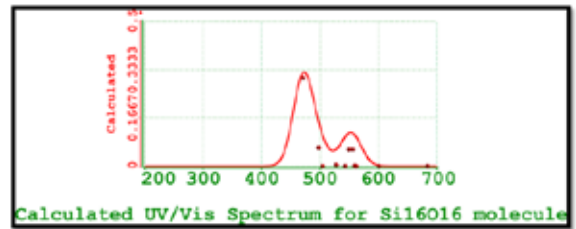


Figure 3. Theoretical PL spectrum calculated for Si16O16 structure.

Units on the horizontal axis are (nm)'s.

This spectrum is correlated with the experimental one of Figure 2.

With regard to the theoretical PL spectrum, Figure 3 exhibits this one, for the films grown at , that was calculated considering the arrangement of a Si16O16 molecule. With this molecular structure, we obtained the PL spectrum which has two remarkable peaks, one of them located at 471 nm with the highest intensity and the other has two located peaks closer at 549.8 and 556 nm. Besides, it was also found an excited state at 683 nm, but its intensity is too negligible or non-detectable.

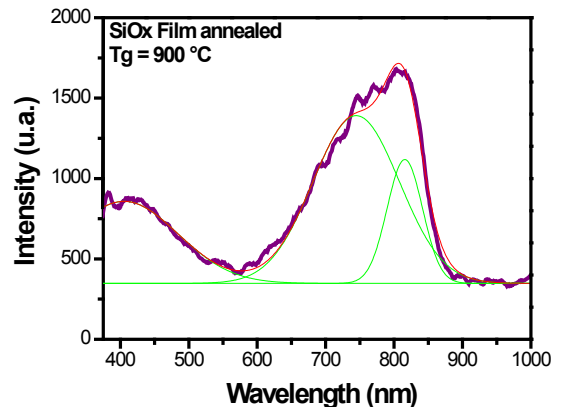


Figure 4. Experimental PL spectrum from a film after a further annealing.

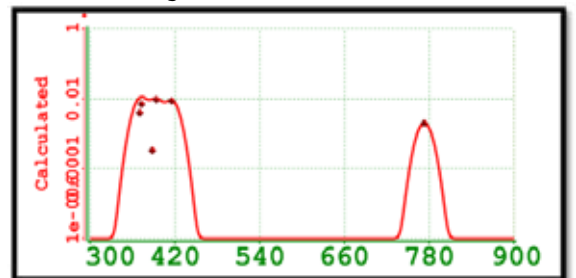
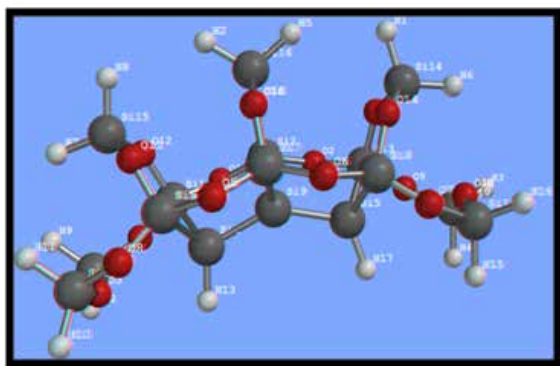


Figure 5. Theoretical PL spectrum correlated to the experimental one of Figure 4 including the annealing effects. This spectrum is reproduced by means of considering the small molecule type Si6O6.

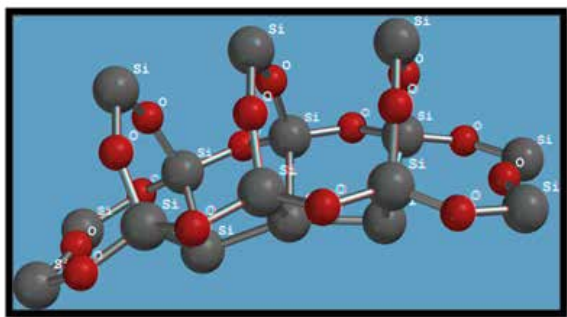
To complement the study of the PL spectrum including annealing effects, in Figure 5 we display results for the theoretical PL spectrum calculated by considering a small molecule type Si6O6. With this molecular structure we predicted excited states emitting in the region from 393.78

to 415.59 nm in addition to a region peaked at 772.8nm which corresponds approximately to the left side of the wide shoulder observed in the experimental spectrum displayed in Figure 4 where the de-convolution curve points out a peak at 749 nm. We emphasize that in this theoretical spectrum is not clear the presence of the peak at 820 nm found in the experimental PL spectrum.

In relation to the study of the configuration of the molecular structure, we present in Figure 6 the two structures corresponding to the case of the film as grown at (top plot) and after a further annealing (bottom plot), both structures correspond to Si<sub>16</sub>O<sub>16</sub> molecule. The structure at the top of the figure consists of 16 hydrogen atoms linked to 8 silicon atoms with tetra valences forming the Si<sub>16</sub>O<sub>16</sub>:H<sub>16</sub> arrangement. On the other hand, in the bottom we display the Si<sub>16</sub>O<sub>16</sub> molecule after annealing. It could be described as a set of seven rings constituted of three member's mini rings each one with two bonds Si-O and a third link Si-Si. There are four mini rings with a semicircular arrangement and the rest is in orthogonal position.



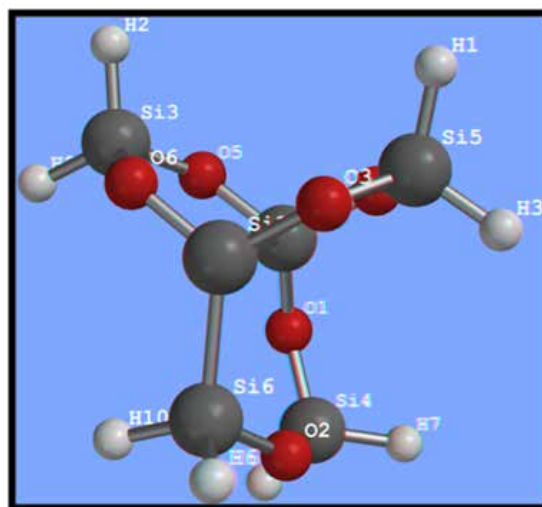
(a)



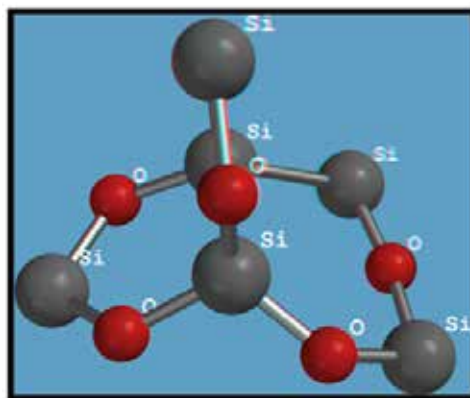
(b)

**Figure 6. Molecular Structure suggested for the film (a) Si<sub>16</sub>O<sub>16</sub>:H<sub>16</sub>, as grown at (b) Si<sub>16</sub>O<sub>16</sub> after a further annealing.**

Regarding the molecular structure proposed for molecule (as grown) it is represented at the top of Figure 7, whereas at the bottom we localize the corresponding molecule after a further annealing. This molecule was proposed for modeling the film after being annealed at 900°C. The structure of this molecule consists only of three mini-rings, two of which are three member rings with two Si-O bonds and one Si-Si bond. The third ring has four silicon atoms with two Si-O bonds and a Si-Si-Si chain. Within the molecule as grown, that is, the six silicon atoms have tetra valence.



(a)



(b)

**Figure 7. Molecular Structure proposed for modeling the film after being annealed at 900°C: (a) As grown is type Si<sub>6</sub>O<sub>6</sub>:H<sub>8</sub>, (b) after annealed is type Si<sub>6</sub>O<sub>6</sub>.**

We now deal with the situation where the growth temperature of films is increased. This implies that the molecular structure should be modified giving rise to another new one with different properties. In Figure 8 we display the experimental PL spectrum measured from a film as grown at a temperature of 1150°C. With the naked eye, wide bands are identified at the right hand and approximately half wide band at the left side. Through de-convolution curves of this spectrum, we can locate the positions of maxima of both bands. The half wide band is peaked around 385 nm and the right band around 690 nm.

Comparatively by Figure 9 we can observe the correlated theoretical PL spectrum calculated for the molecule. With this molecular structure, we have predicted a PL spectrum having only two bands where the half left band possesses the highest intensity being peaked at 380 nm, and the other one with lower intensity and its maxima correspond to an excited state of emission at 699 nm. In this case, we did not look for triplets for the molecule, taking for granted that if they exist they would have a negligible intensity.

Furthermore, the molecular structures suggested for the molecule are represented in Figure 10. The top structure corresponds to the as-grown molecule. In the arrangement of this structure we figure out that there are 12 hydrogen atoms joined to six silicon ones with tetra valence. The "backbone of this mol-

ecule" is a silicon atom joined to four silicon atoms shaping a tetrahedral arrangement, with six mini rings constituted where five of them have four silicon atoms and two Si-O bonds each one and a Si-Si-Si chain. The sixth mini -ring has only one Si-O bond and a large silicon chain Si-Si-Si-Si.

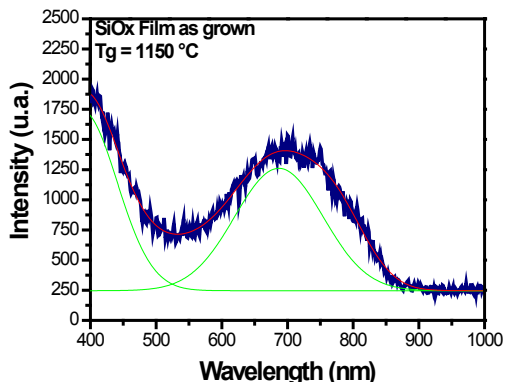


Figure 8. Experimental PL spectrum of a film grown at 1150°C.

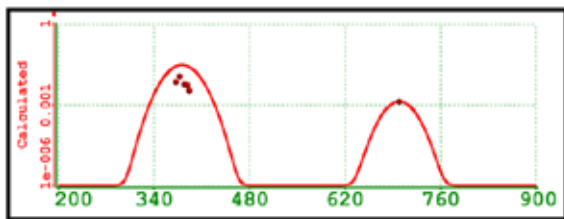
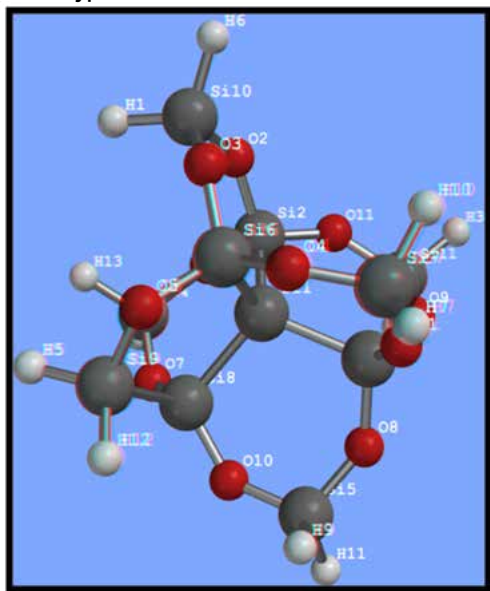
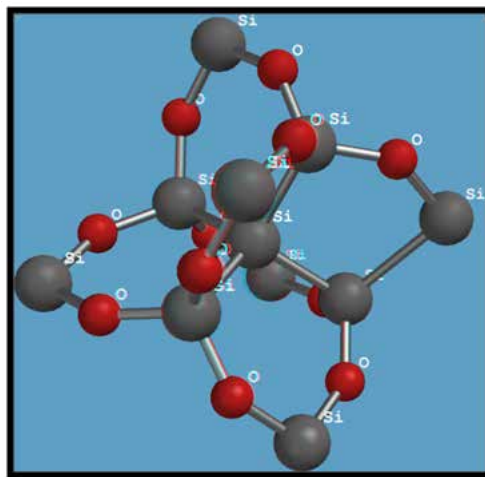


Figure 9 Correlated theoretical PL spectrum of Figure 8. In this case the film is modeled with a molecular structure of type Si11O11 molecule.



(a)



(b)

Figure 10. Molecular Structure suggested. (a) as grown it corresponds to Si11O11:H12 arrangement, (b) After annealed the molecular arrangement is type Si11O11.

### 3.3 FTIR spectra of the thin films

In order to get a more complete evaluation of the optical and structural properties of SRO, we now proceed to make a theoretical analysis of Fourier Transform Infrared (FTIR) spectroscopy. In practice, FTIR is a technique used for structural characterization of materials with which is possible to study atomic bonds between elements that are present in a given film. The various bonds are manifested as different absorption bands which lie in different wavelength ranges. The position and shape of these bands are related to the density, stoichiometry and the nature of the bond primarily. The infrared energy causes vibrational motion of atoms in a molecule identified as rocking, stretching, wagging and bending when they interact with such energy. A fraction of the incident radiation is absorbed at specific wavelengths. A molecule must vibrate so that there is a displacement from the electrical center and absorbed radiation in the infrared region, i.e., there must be a change in the dipole moment.

In Figure 11, we display the experimental FTIR spectrum of a film grown at 900°C. According to Aydinly et al. they have associated these vibrational frequencies as indicated in Table 2. In such Table 2, we make comparisons between vibrational frequencies as found experimentally (Figure 11) and theoretical frequencies as obtained in this report when considering a molecule in addition to being identified with the different vibrational modes reported in literature. Particularly, the experimental frequencies at 654 cm<sup>-1</sup> and 875 cm<sup>-1</sup>, in Figure 11, have been associated as reported in literature to Si-H vibrational frequencies. Comparing these latter frequencies with those found by our theoretical calculations we find discrepancies since we observed from Table 2 that such theoretical frequencies which are attributable to Si-H vibrational frequencies are located at 652 cm<sup>-1</sup> and 885 cm<sup>-1</sup> which are, in our case, due to Si-Si and Si-O bonds

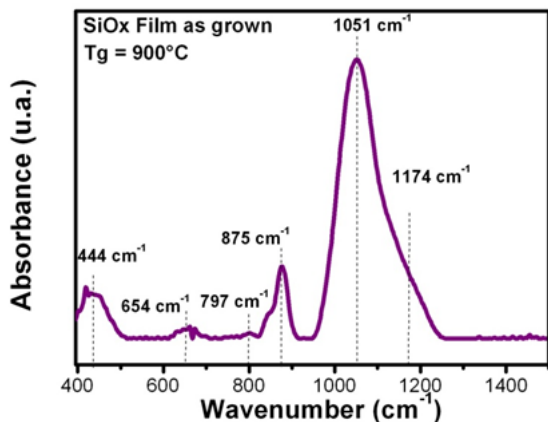


Figure 11. Experimental FTIR spectrum from a film as grown at 900°C.

Apart from discrepancies in their values between experimental and theoretical frequencies, we also find differences between their associated intensities as is evident from Figure 12 at the top FTIR spectrum (a) when is compared with Figure 11. Two very remarkable differences in their intensities are found in peaks located at 875 cm<sup>-1</sup> and 1051 cm<sup>-1</sup> in the experimental FTIR spectrum and their correlated theoretical values located in Figure 12 (a) approximately at 885 cm<sup>-1</sup> and 1058 cm<sup>-1</sup>, in fact, if we observe carefully theoretical and experimental intensities are inverted in magnitude. On the other hand, we stress that plot in Figure 12 (a) corresponds to a Gaussian curve fitted to FWHH=40, whereas plot in Figure 12(b) corresponds to a Gaussian curve fitted to FWHH=80. We can appreciate clearly that the difference in FWHH values gives rise that the peak at 1058 cm<sup>-1</sup> in Figure (a) is transformed into a shoulder of the peak at 885 cm<sup>-1</sup> as is shown in Figure 12 (b). The effect of varying FWHH to higher values has brought as a consequence that FTIR spectrum becomes more intense, Figure 12(b), it means physically as the film were thicker in addition to this FTIR spectrum resembles more to the experimental one of Figure 11 although persists discrepancies in wavenumbers.

Table 2. Comparison of vibrational frequencies observed experimentally in a film as grown at 900 °C vs. calculated FTIR spectrum for a Si16O16 molecule.

wavenumber cm <sup>-1</sup> . SiO <sub>x</sub> Film as grown from 900°C to 1150°C					
Associated in literature to	Si-O rocking	Si-H wagging	Si-O bending	Si-H bending	Si-O stretching
Experimental	429-444	645-654	797-810	875-885	1048-1064
Calculated using DFT		Si-Si Bending in Si <sub>16</sub> O <sub>16</sub> molecule		Si-O in "external rings"	
Calculated	438	652	794	885	1058

Now, we consider important to study the influence of annealing process on FTIR spectra. For this, we focus on a thin film deposited at 900°C with a further annealing, normally carried out in the (1100-1150)°C range. Figure 13 displays the experimental FTIR spectrum for this sample. It is worthwhile to mention that after the films have been heat-treated (annealed), the FTIR spectrum peaks corresponding or associated to Si-H vibrational frequencies disappear. Also, the uppermost peak which corresponds to Si-O stretching mode (1051 cm<sup>-1</sup>) is considerably shifted to higher frequencies (1082 cm<sup>-1</sup>) indicating a phase separation. It is possible then, for example, that a molecule like SiH4 or SiH2 (it depends mainly on both time and annealing temperature. On

the other hand, it has been reported that amorphous silicon (a-Si) as well as crystalline one (c-Si) could be identified by Raman spectroscopy. A broad band around ~ 480 cm<sup>-1</sup> is typically associated to a-Si, while bulk silicon has a sharp intensity peak around 521 cm<sup>-1</sup>. As to SiH4, it is found that intensity peaks are shifted to smaller wavenumbers where this change is a function of decreasing size, this event has been extensively attributed to quantum confinement effects. For example, in Figure 14 which corresponds to a theoretical Raman spectrum that we have calculated for a molecule suggested, we can clearly identify frequencies at 460 cm<sup>-1</sup> and 508 cm<sup>-1</sup> respectively.

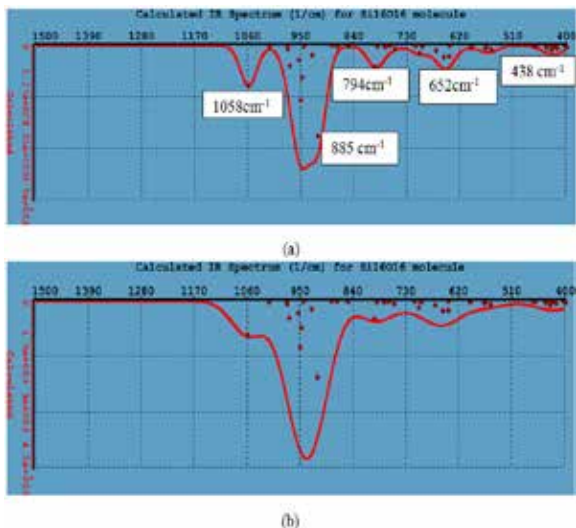


Figure 12. Theoretical FTIR spectra calculated using DFT for a Si16O16 molecule. (a) Vibrational frequencies found in this spectrum, when are correlated to those of Figure 11, show discrepancies. This plot corresponds to a Gaussian curve fitted to FWHH=40 and (b) FWHH=80.

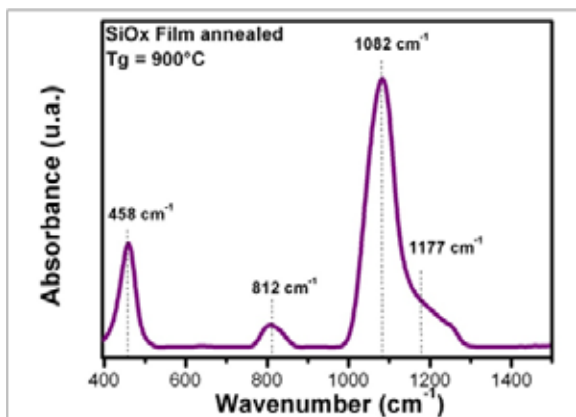
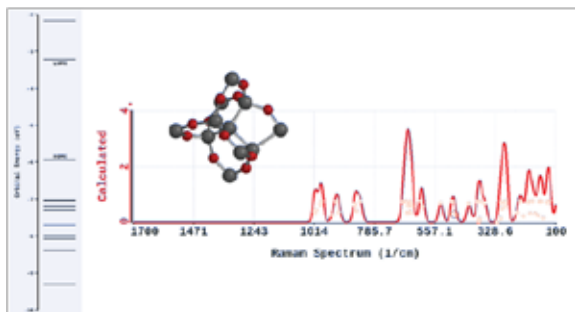


Figure 13. Experimental FTIR spectrum from a thin film after a further annealing.



**Figure 14. Theoretical Raman spectrum calculated for [Si11011] configuration. We identify in the center of Figure the atomic structure and the left side inset displays the Orbital Energy in units of (eV).**

We have explained previously that the molecule has two chains, one is type Si-Si-Si and the other is a larger chain type Si-Si-Si-Si (tetragonal arrangement shape).

On the other hand, we evaluated four isomers for Si18 agglomerates. These correspond to isomers identified as 18A, 18B, 18C and 18D from which isomer 18D did not achieve convergence consequently information about it is not available. Table 3 contains information about isomer 18A, B and C. We can appreciate that isomer 18C is not the most stable because it has the highest energy. Contrary, the isomer Si18A(18A) possesses the lowest energy (a difference of 0.96 eV as indicated in third column) by this reason is the most stable of all. Other parameters of interest were calculated such as, the bandgap, the dipole moment, the polarizability and the ovality.

With regard to cluster, four low-lying isomers were considered. The elongated isomer 18A has the lowest-energy at the HF/6-31G\* level of theory. Moreover, the isomer 18A has its structure similar to the ground-state structure predicted by Rata et al. It contains a magic-number-cluster unit and a hexagonal chair unit. A slight structural perturbation to this isomer followed by a geometry relaxation gives isomer 18 B with symmetry. Both 18B and 18C with symmetry contain tri-capped-trigonal-prism unit and are also very viable in stability compared to 18A because of the calculated difference in energy was 0.92 and 0.96 eV respectively. Isomer 18D is a new isomer with high symme-

try but relatively high energy. It is composed of two capped tetragonal anti-prisms, and we did not obtain convergence at HF/6-31G\* level of theory for this isomer. We also observe from Table 3 the predicted wavelength of the highest emission intensity corresponding to each isomer under the following order: 552.4 nm for 18A isomer, 692.8 nm for isomer 18B and 1732.7 nm for isomer 18C.

We find out the information given in Figure 15. There, with the naked eye, we locate at the top of the figure the FTIR spectrum and at the bottom of the one the PL spectrum both corresponding to isomer 18C calculated using DFT. In the PL spectrum is outstanding the appearance of the uppermost intensity peak predicted at 679.9 nm according to our theoretical approach. Finally, we can see in the middle of Figure 15 the suggested molecular structure corresponding to the isomer. Furthermore, the top graph in Figure 15 represents the FTIR spectrum of the isomer 18C, it presents the two most intense peaks at the vibrational frequencies around of 179 and 262  $\text{cm}^{-1}$  where we point out that two remaining calculated wavenumbers were imaginary. The three smallest peaks appear at frequencies around of 305, 390 and 434  $\text{cm}^{-1}$ .

**Table.3 Parameters calculated for isomers Si18.**

Isomer	Energy (au)	Rel. E (eV)	Band gap eV	Dipole debye	Polarizability	Wavelength nm, corresponding to highest emission intensity	Ovality
18A	-5210.83526	0.00	2.2550	2.84	75.20232	552.447567	1.25050
18B	-5210.80158	0.92	1.3883	0.04	75.20910	692.813713	1.25806
18C	-5210.80010	0.96	1.3232	0.01	75.21392	1732.74488 (not shown in figure 15)	1.25816

## REFERENCE

- Werwa, E., & Seraphin, A. A., & Chiu, L. A., Zhou, C. & Kolenbrander, K. D. (1994). Synthesis and processing of silicon nanocrystallites using a pulsed laser ablation supersonic expansion method. *Applied physics letters*, 64(14), 1821-1823. Retrieved from | <http://dx.doi.org/10.1063/1.111766> | X.X. Wang, & J.G. Zhang, & L. Ding, & B.W. Cheng, & W.K. Ge, & J. Z. Yu & Q. M. Wang. (2005). Origin and evolution of photoluminescence from Si nanocrystals embedded in a SiO<sub>2</sub> matrix. *Phys. Rev. B*, 72, 195313. 1-6 Retrieved from <http://link.aps.org/doi/10.1103/PhysRevB.72.195313> | Canham, L. T. (1995). Luminescence bands and their proposed origins in highly porous silicon. *Physica status solidi (b)*, 190(1), 9-14. Retrieved from | <http://dx.doi.org/10.1002/psb.2221900102> | F. G. Bell, & L. Ley, (1988) Photoemission study of SiOx (0<math>x</math>2) alloys. *Phys. Rev. B*, 37, 8383-8893. | H. R. Philipp, (1971) Optical properties of non-crystalline Si, SiO, SiOx and SiO<sub>2</sub>. *J. Phys. Chem. Solids*, 32(8), 1935-1945. | Y. N. Novikov, & V. A. Gritsenko, (2011) Short-range order in amorphous SiOx by X ray photoelectron spectroscopy. *J. Appl. Phys.*, 110, 014107.1-6. Retrieved from | <http://dx.doi.org/10.1063/1.3606422> | Ristic, D., & Ivanda, M., & Speranz, G., & Siketic, Z., & Bogdanovic-Radovic, L., & Marcic, M., & Ristic, M., & Gamulin, O., & Music, S., & Furic, K., & C. Righini, G., & Ferrari, M. (2012). Local site distribution of oxygen in silicon-rich oxide thin films: A tool to investigate phase separation. *J. Phys. Chem. C*, 116, 10039-10047. Retrieved from <http://pubs.acs.org/doi/abs/10.1021/jp301181y> | N. D. Espinosa-Torres, & J. F. Flores-Gracia, & J. A. Luna-López, & D. Hernández de la Luz, & J. Martínez-Juárez. (2014). Computer Simulation of Luminescence in Silicon Rich Oxide Thin Films Arising From silicon-Oxygen Bonds. *International Journal of Scientific Research*, 3(7), 82-92. | H. Wiesmann, & A. K. Ghosh, & T. McMahon, & M. Strongin, (1979) a-Si:H produced by high-temperature thermal decomposition of silane. *J. Appl. Phys.*, 50(5), 3752-3754. | Fang, Y. C., & Li, W. Q., & Qi, L. J., & Li, L. Y., & Zhao, Y. Y., & Zhang, Z. J., & Lu, M. (2004). Photo-luminescence from SiOx thin films: effects of film thickness and annealing temperature. *Nanotechnology*, 15, 495-500. <http://dx.doi.org/10.1088/0957-4484/15/5/016> | Aceves, M., & Malik, A., & Murphy, R. (2001). The FTO/SRO/Si structure as a radiation sensor. *Research Signpost*, ISBN: 81-7736-067-1, 1-25. | Matsumoto, Y., & Godavarthi, S., & Ortega, M., & Sánchez, V., & Velumani, S., & Mallick, P.S. (2011). Size modulation of nanocrystalline silicon embedded in amorphous silicon oxide by Cat-CVD. *Thin Solid Films*, 519, 4498-4501. | Banerjee, C., & Sritharathikhum, J., & Yamada, A., & Konagai, M. (2008). Fabrication of hetero-junction solar cells by using microcrystalline hydrogenated silicon oxide film as an emitter. *J. Phys. D: Appl. Phys.*, 41, 185107.1-5. Retrieved from | <http://iopscience.iop.org/0022-3727/41/18/185107> | Gritsenko, V. A., & Xu, J. B., & Kwok, R. W. M., & Ng, Y. H., & Wilson, J. H. (1998). Short Range Order and the Nature of Defects and Traps in Amorphous Silicon Oxynitride Grown by the Mott Rule. *Phys. Rev. Lett.* 81, 1054-1057. Retrieved from | <http://link.aps.org/doi/10.1103/PhysRevLett.81.1054> | Philipp, H. R. (1972). Optical and bonding model for non-crystalline SiOx and SiOxNy materials. *Journal of Non-Crystalline Solids* 8(10), 627-632. Retrieved from <http://www.sciencedirect.com/science/article/pii/002230972902025> | Pankove, J.I. (1971). Optical Processes in Semiconductors. N.Y., U.S.A. Dover Publications, Inc. | Luna López, J. A., & Carrillo López, J., & Vázquez Valerdi, D. E., & García Salgado, G., & Díaz Becerril, T., & Ponce Pedraza, A., & Flores Gracia, F. J. J. (2012). Morphological, compositional, structural, and optical properties of Si-nc embedded in SiOx films. *Nanoscale Research Letters* 7, 604. 1-10. <http://www.nanoscaleslett.com/content/7/1/604> | D. E. Vázquez Valerdi, J. A. Luna López, J. Carrillo López, G. García Salgado, A. Benítez Lara & N. D. Espinosa Torres. Compositional and optical properties of SiOx films and junctions (SiOx/SiOy) deposited by HFCVD. *Nanoscale Research Letter*. To be published. | Ay F & Aydinly A. (2004). Comparative investigation of hydrogen bonding in silicon based PECVD grown dielectrics for optical waveguides. *Opt. Mater.*, 26, 33-46. | Kiebach, R., & Luna-López, J. A., & Osvaldo Dias, G., & Aceves-Mijares, M., & Willibrordus Swart, J. (2008). Characterization of Silicon Rich Oxides with Tunable Optical Band Gap on Sapphire substrates by Photoluminescence, UV/Vis and Raman Spectroscopy. *J. Mex. Chem. Soc.*, 52(3), 212-218. | Rata, I., & Shvartsburg, A. A., & Horoi, M., & Fraunheim, Th., & Siu, K. W. M., & Jackson, K. A. (2000). Single-Parent Evolution Algorithm and the Optimization of Si Clusters. *Phys. Rev. Lett.*, 85, 546-549. <http://link.aps.org/doi/10.1103/PhysRevLett.85.546> |